Saudi Journal of Biological Sciences 28 (2021) 7160–7174

Contents lists available at ScienceDirect

Saudi Journal of Biological Sciences

journal homepage: www.sciencedirect.com

Ultrastructural study of collagen fibrils, proteoglycans and lamellae of the cornea treated with iontophoresis – UVA cross-linking and hypotonic riboflavin solution

Turki Almubrad [a], Rita Mencucci [c], Adrian Smedowski [b,c], Ramachandran Samivel [a], Essam Almutleb [a], Aljohara Alkanaan [a], Adnan Ali Khan [a], Ali Masmali [a], Saeed Akhtar [a,*]

[a] Cornea Research Chair, Department of Optics and Vision Sciences, College of Applied Medical Science, King Saud University, Riyadh, Saudi Arabia
[b] Department of Physiology, Faculty of Medical Sciences in Katowice, Medical University of Silesia, Katowice, Poland
[c] Department of Oto-Neuro-Ophthalmology Surgical Sciences, Eye Clinic, University of Florence, Italy

ARTICLE INFO

Article history:
Received 25 March 2021
Revised 31 July 2021
Accepted 3 August 2021
Available online 10 August 2021

Keyword:
Collagen fibrils
Proteoglycans
Cornea
Iontophoresis
Ultraviolet A

ABSTRACT

To investigate the effects of iontophoresis–ultraviolet A (UVA) cross-linking (CXL) with hypotonic riboflavin solution on the ultrastructural changes in the lamellae, collagen fibrils (CFs), and proteoglycans (PGs) in the central and peripheral stroma of the human corneal buttons. The iontophoresis method was used for the *trans*-epithelial application of hypotonic riboflavin in *ex vivo* corneal culture for 5 min. The corneas were irradiated using three methods: ***Group 1 (G1)***, a UVA irradiance of 3 mW/cm^2 for 30 min; ***Group 2 (G2)***, a UVA irradiance of 10 mW/cm^2 for 9 min; ***Group 3 (G3)***, without UVA irradiation. Three untreated corneas were used as controls (***G0***). After the CXL procedure, the corneas were processed for electron microscopy. The CF diameter and PGs in each sample were analyzed using the iTEM program. The keratocyte organelles and stromal architecture in the peripheral cornea were better preserved than those in the central cornea. In *G1* and *G2*, the mean CF diameter in the peripheral cornea was significantly higher than that in the central cornea. In *G3*, the CF diameter in the central cornea was significantly larger than that in the peripheral cornea. Furthermore, differences in PG area size were observed between the central and peripheral corneas in all groups. Riboflavin + UVA application at 3 mW/cm^2 for 30 min and 10 mW/cm^2 for 9 min was a suitable method of CXL; however, 3 mW/cm^2 for 30 min improved the organization and size of the collagen fibrils. CXL treatment applied at the periphery was more effective than that applied at the center.

Contents

1. Introduction . . . 7161
2. Methods . . . 7161
   2.1. Ethics . . . 7161
   2.2. Study groups . . . 7161
   2.3. Iontophoresis procedure . . . 7162
   2.4. Electron microscopy method . . . 7162
3. Results . . . 7162

* Corresponding author.
E-mail address: Akhtars@ksu.edu.sa (S. Akhtar).

Peer review under responsibility of King Saud University.

Production and hosting by Elsevier

https://doi.org/10.1016/j.sjbs.2021.08.019
1319-562X/

3.1. Ultrastructural changes of normal and CXL-treated corneas . . . 7162
3.2. CF diameter and interfibrillar spacing of the anterior stroma of normal and CXL-treated corneas . . . 7166
3.3. Mean PG area and density of normal and CXL-treated corneas . . . 7166
4. Discussion . . . 7166
4.1. Ultrastructural changes in the center and periphery of corneas from the analyzed groups . . . 7168
4.2. Within the same cornea of G1, G2, and G3: CF diameter and interfibrillar spacing in the center and periphery . . . 7168
4.3. Among the corneas of G1, G2, and G3: CF diameter and interfibrillar spacing . . . 7168
Declaration of Competing Interest . . . 7173
Acknowledgments . . . 7173
References . . . 7173

1. Introduction

The cornea is the most anterior transparent layer of the eye and the main ocular refractive medium (Nautscher et al., 2016). Corneal transparency is maintained by the uniform distribution of collagen fibrils (CFs) and the organization within the stromal lamellae, which are regulated by corneal proteoglycans (PGs) (Cheng and Pinsky, 2013; Ho et al., 2014). Changes in the expression of PGs were described to be associated with corneal transparency loss and change in corneal curvature leading to visual deterioration (Bredrup et al., 2005; Pellegata et al., 2000).

Keratoconus (KC) is a bilateral asymmetrical corneal disease in which progressive thinning and bulging impair vision (Rabinowitz, 1998). Investigation of CFs and PGs in the cornea of individuals with KC suggests alterations in the arrangement of CFs and PGs (Akhtar et al., 2011, 2008; Chaerkady et al., 2013; Fullwood et al., 1992; Funderburgh and Conrad, 1990; Sawaguchi et al., 1991; Wollensak and Buddecke, 1990). Wollensak et al. (2003a) have pioneered the riboflavin–ultraviolet A (UVA) cross-linking (CXL) treatment for KC. The CXL treatment enhances the biomechanical properties and stabilize the interfibrillar and intrafibrillar spaces of the cornea to inhibit the progression of KC (Wollensak et al., 2011, 2003b). Presently, CXL is widely used in treating progressive KC and other corneal ectatic disorders (Belin et al., 2018; Mazzotta et al., 2018). Studies on the human cornea have shown that CXL treatment restores epithelial and anterior stromal keratocytes and enhances the architecture of CFs and flattens undulating lamellae (Akhtar et al., 2013; Mazzotta et al., 2008; O'Brart et al., 2015).

The accelerated CXL protocol was developed following the photochemical law of reciprocity (also known as the Bunsen–Roscoe law) to reduce treatment time. According to the law, the total irradiation and photochemical effect will be same if the irradiation time is reduced while increasing the irradiance (O'Brart et al., 2015). Wernli et al.'s assessment of *ex vivo* porcine corneas treated with different irradiances for a duration ranging from 1 min to 30 min has revealed significant stiffening after the application of high irradiances up to 45 mW/cm^2 (Wernli et al., 2013). Herber et al (2018) compared the effect of "higher peripheral intensity" profile setting and standard "top hat" profile with accelerated CX. The comparison of the two profiles showed that the effect of "higher peripheral intensity" was more pronounced compared to those in the "top hat" profile, on the topographic and tomographic parameters of the keratoconus cornea (Herber et al (2018). Recently, the role of oxygen in relation to depth of the corneal stroma during CXL treatment and its depletion with depth of the corneal stroma was discussed by Seiler et al. (2020).

Studies have shown that in the cornea of individuals with KC, the undulating lamellae changed into parallel running lamellae, and the diameter of CFs increased with regular interfibrillar spacing after CXL treatment (Akhtar et al., 2013; Mencucci et al., 2010; Wollensak et al., 2004b). CXL treatment not only affects the stromal collagen but also affects the synthesis of PGs. Following their assessment of normal, KC, and CXL-treated KC corneas, Akhtar et al., (2013) have revealed that the PGs in the CXL-treated corneas have an organization similar to that of normal corneas. The *in vitro* assessment of normal and KC fibroblasts treated with CXL by Sharif et al., (2018) has suggested that CXL treatment significantly enhances the expression of the PGs mimican, decorin, and lumican but reduces the expression of keratocan. Few studies on the effects of iontophoresis corneal CXL on corneal biomechanical rigidity, on morphological changes of the cornea, and on keratocytes have been conducted (Manetti et al., 2017; Mencucci et al., 2015; Vinciguerra et al., 2014). In this study, we investigated the *ex vivo* effects of different UVA irradiances on the ultrastructure and organization of CFs and PGs in the human corneal stroma treated with hypotonic riboflavin solution by iontophoresis.

2. Methods

2.1. Ethics

The ethical approval for corneal tissue procurement and use was granted by the Local Ethical Committee of King Saud University, Saudi Arabia. All experiments were performed according to the guidelines of "Standing Committee For Research Ethics on Living Creatures (SCRELC)" Saudi Arabia. The policy is available at https://www.uod.edu.sa/sites/default/files/resources/implementing_regulations_0.pdf.

2.2. Study groups

Twelve anonymous corneal buttons (8.5 mm in diameter), used in this study, were obtained from the Eye Bank of Mestre (Italy) and cultured *ex vivo* to maintain their viability. The *ex vivo*-cultured corneas were soaked in a commercial formulation of hypotonic riboflavin (Ricrolin$^{+®}$, Sooft, Montegiorgio, FM, Italy) intracorneally delivered using an iontophoresis device and irradiated by a UVA source (VEGA CBM x-linker, C.S.O, Florence, Italy) (Mencucci et al., 2015). The Ricrolin$^{+®}$ riboflavin solution for ion CXL contains 0.14% riboflavin phosphate sodium salt, 0.05% trisaminomethane, 0.1% ethylenediaminetetraacetic acid, 0.21% $NaHPO_4 2H_2O$, and 0.36% $NAH_2PO_4 2H_2O$, ensuring rapid transepithelial penetration.

The corneas were divided into four groups (three corneas in each group) according to the time of exposition to riboflavin and applied UVA irradiance: Group 1 (***G1***) comprised three corneas treated with a Ricrolin$^{+®}$riboflavin formulation using an iontophoresis device for 5 min and an UVA irradiance of 3 mW/cm^2 for 30 min; Group 2 (***G2***) comprised three corneas treated with a Ricrolin$^{+®}$riboflavin formulation using an iontophoresis device for 5 min and an UVA irradiance of 10 mW/cm^2 for 9 min; Group 3 (***G3***) comprised three corneas treated with a Ricrolin$^{+®}$riboflavin formulation using an iontophoresis device for 5 min with no sub-

sequent UVA irradiation; and Group 0 (***G0***) comprised three untreated corneas.

2.3. Iontophoresis procedure

The application of riboflavin using an iontophoresis device and the UVA radiation method have been described by Mencucci et al. (2015). The irradiated area was 9 mm and the radius of the extraction for the periphery was 4 mm. Briefly, the main components of the iontophoresis device used in this study are the power supply (I-ON XL, Sooft) and two electrodes. The human corneas were placed on an artificial anterior chamber for *ex vivo* culture (Barron artificial anterior chamber; Katena, Denville, NJ, USA) equipped with two pressure tubes connected to a perfusion line, allowing culture media circulation during the experiment. The negative electrode, made of an 8-mm-diameter stainless-steel grid inserted into an annular suction rubber ring, was placed into the cup at a minimal distance of 5 mm from the cornea. The device was irrigated with approximately 0.5 mL of riboflavin solution from the open proximal side until the electrode was completely immersed. The positive electrode was a stainless-steel wire connected to the artificial anterior chamber underneath the cornea. In clinical settings, the positive electrode is usually a conductive patch applied to the patient's skin. A constant current of 1.0 mA was applied from the power generator. Iontophoresis continued for 5 min, and hypotonic riboflavin drops were applied to the cornea every 5 min throughout the procedure.

2.4. Electron microscopy method

After the CXL has been completed, the corneas were removed from the artificial chamber and washed with a sterile phosphate buffer saline to remove riboflavin residues. The corneas were kept in the storage medium Eusol C (Alchimia, Padova, Italy) at 4 °C for 48 h. The corneas were removed from the storage medium Eusol C and fixed in a mixture of 4% paraformaldehyde and 0.5% glutaraldehyde in 0.1M phosphate buffer for 24 h at 4 °C and washed in 0.1M phosphate buffer. For electron microscopy, each cornea was cut into two halves: one half was fixed in 2.5% glutaraldehyde containing 0.05% Cuprolinic Blue (BDH Ltd, Poole, UK) using a critical electrolyte concentration mode to analyze the PGs. The other half was fixed in 2.5% glutaraldehyde and osmium tetroxide for fibrillar and lamellar analysis (Akhtar et al., 2016). Then, the tissue was dehydrated in a graded series of ethanol (50%–100%) and acetone and then infiltrated with Spurr resin. Each corneal half was cut into four conical quarters, and each quarter was further cut into halves: the conical central and peripheral parts. The central part consisted of 1 mm from the center, and the peripheral part consisted of 1 mm from the margin of the cornea. The tissue was embedded in Spurr resin for 8 h at 70 °C. During embedding in the green mold, the conical central part of the conical quarter was faced toward the cutting surface to obtain ultrathin sections from the center, and the marginal part of the peripheral quarter was faced to the cutting surface to obtain ultrathin sections from the periphery. The total number of osmium-treated blocks was 24: 12 central and 12 peripheral blocks. The total number of cuprolinic blocks was 24 as well: 12 central and 12 peripheral blocks.

An RMC microtome was used to cut ultrathin sections (70 nm) collected on 200 mesh copper grids. Ten grids were made from each block and stained with 2% uranyl acetate for 10 min and lead citrate for 10 min. The best ultrathin sections from three grids from each block were examined under the JEOL 1400 (Jeol Ltd, Akishima, Japan) transmission electron microscope (TEM), and digital micrographs were captured using an 11-megapixel Quemesa camera and iTEM software. Five images from each section were taken at different parts of the anterior stroma, and the best three images were chosen to analyze CFs or PGs. In total, 480 sections were collected on grids, and 2400 digital images were taken.

The iTEM software was used to generate and analyze color-coded images of the digital micrographs in addition to measuring the following parameters: CF diameter, CF interfibrillar spacing, PG area, and PG density. Finally, data were exported from the software into Microsoft Excel (Microsoft Corporation, Washington, USA) spreadsheets and analyzed using Statistical Package for the Social Sciences, version 18 (IBM Corp., Armonk, NY, USA). Using the Mann–Whitney *U* test, the following variables were compared between the groups: mean CF diameter and spacing and mean PG density and area.

3. Results

3.1. Ultrastructural changes of normal and CXL-treated corneas

In the control group, the lamellae, CFs, and PGs were well-organized at the center and periphery of the cornea. The anterior stromal lamellae were interlaced, whereas the lamellae at the middle and posterior stroma were running parallel to each other (Fig. 1A, B). The keratocytes contained normal nucleus and cell organelles.

In the peripheral stroma in *G1*, the Bowman layer (BW) was well-organized and appeared similar to a healthy BW. A large number of CFs was observed emerging from the BW and entering the lamellae of the anterior stroma. The anterior stromal lamellae were interconnected (interlaced) with each other but contained minute electron-lucent spaces (Fig. 1C, D). Most keratocytes contained normal cell organelles and a large nucleus, but some keratocytes were surrounded by electron-dense materials (Fig. 1E). In the central stroma in *G1*, some lamellae were folded (Fig. 1F). A large number of electron-dense spaces were observed in the BW and anterior stroma, and keratocytes showed signs of damage leaving large vacuoles (Fig. 1G, H).

In *G2*, the BW contained electron-dense patches and long-isolated CFs in both the central and peripheral stroma (Fig. 2A). The anterior stromal lamellae were interlaced with each other but contained electron-lucent spaces and electron-dense patches between loosely arranged fibrils in both the peripheral and central stroma (Fig. 2B). The keratocytes in the peripheral stroma contained large nuclei and cell organelles, whereas those in the central stroma were damaged and contained lysosomes (Fig. 2C, D). They did not have visible nuclei or cell organelles and contained large electron-lucent vacuoles (Fig. 2D).

In *G3*, the structures of the BW and lamellae were similar in both the central and peripheral stroma. In both the peripheral and central corneas, the BW had isolated long CFs and numerous electron-lucent spaces (Fig. 2E, F). The CFs below the BW were running in various directions enclosing large electron-lucent spaces (Fig. 2G). This may have been due to the high amount of water separating the CFs, which created electron-lucent spaces without signs of cellular damage. The keratocytes in both the central and peripheral stroma had large nuclei and cell organelles. In the central stroma, vertically running lamellae were observed connecting to the two parallel running lamellae (Fig. 2H).

The microfilaments within the CFs were well-defined and normally distributed in both the center and periphery of normal corneas of the control group (Fig. 3A, B). The ultrastructure within the CFs at the periphery and center was different in all groups. In *G1*, the CFs in the periphery contained well-differentiated microfilaments surrounding a central lucent space, whereas in the central part, the microfilaments were randomly distributed (Fig. 3C, D). In addition, some CFs in the center were damaged and fused (Fig. 2D). In *G2*, a large number of CFs were damaged (Fig. 3E, F, arrowhead),

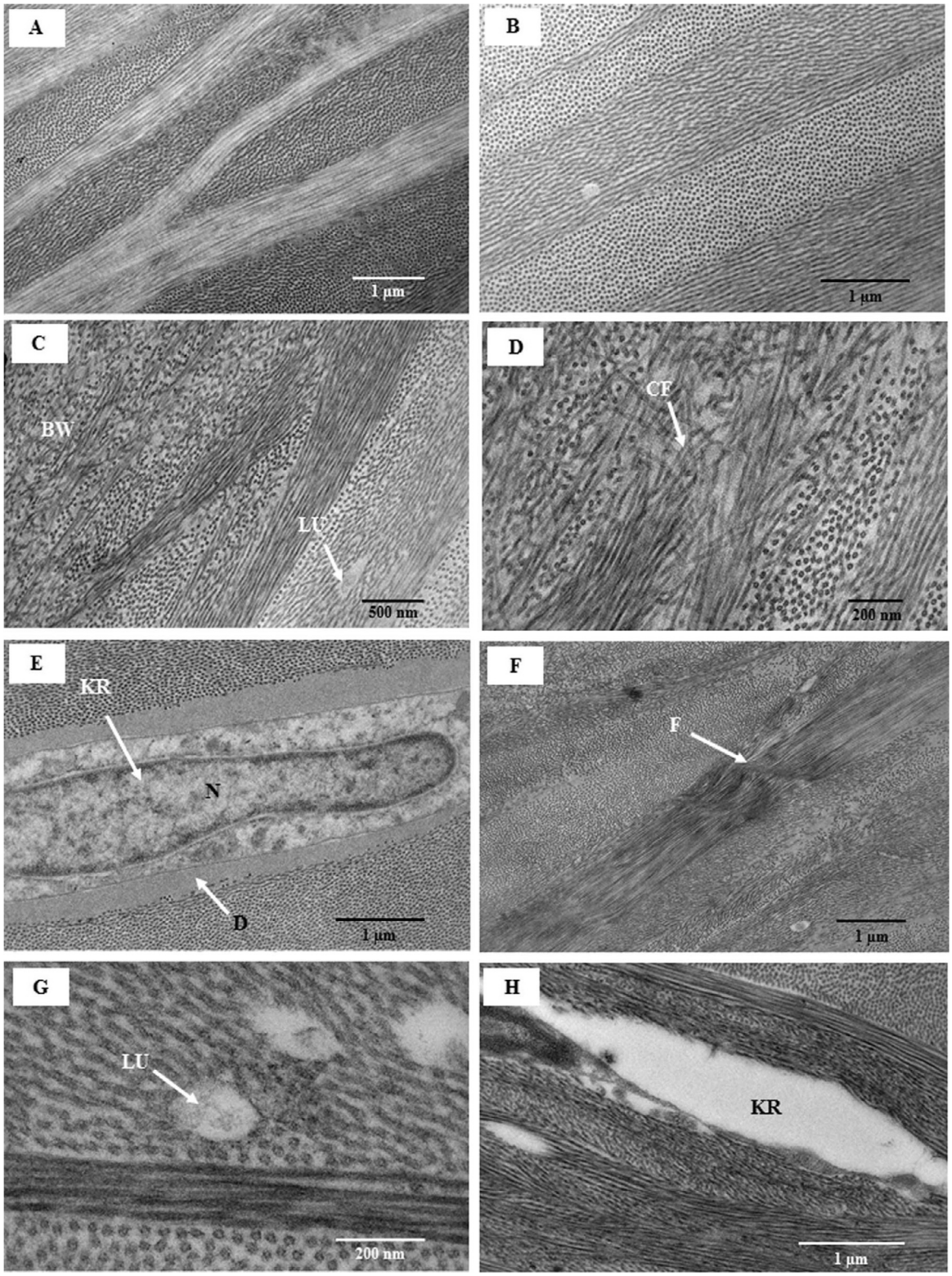

Fig. 1. Electron micrograph of the periphery and center of normal and *Group 1* corneas. **A**) Part of the normal central cornea showing interconnectivity of the lamellae in the anterior stroma. **B**) Part of the normal central cornea showing parallel running lamellae in the middle stroma. **C**) Part of the peripheral *Group 1* cornea showing normal the Bowman layer (BW), interlacing lamellae, and electron-lucent vacuoles in the collagen fibrils (CFs) of the anterior stroma. **D**) Part of the anterior stroma of *Group 1* peripheral cornea showing the emergence of CFs from the BW. **E**) Part of the anterior stroma of *Group 1* peripheral cornea showing keratocytes with large nuclei surrounded by an electron-dense material. **F**) Part of *Group 1* central cornea showing folded lamellae in the anterior stroma. **G & H**) Part of *Group 1* central cornea showing electron-lucent spaces and degenerated keratocytes in the anterior stroma.BW, Bowman layer; CF, collagen fibril; D, electron-dense material; F, folded lamellae; KR, keratocyte; LU, lucent spaces; N, nucleus.

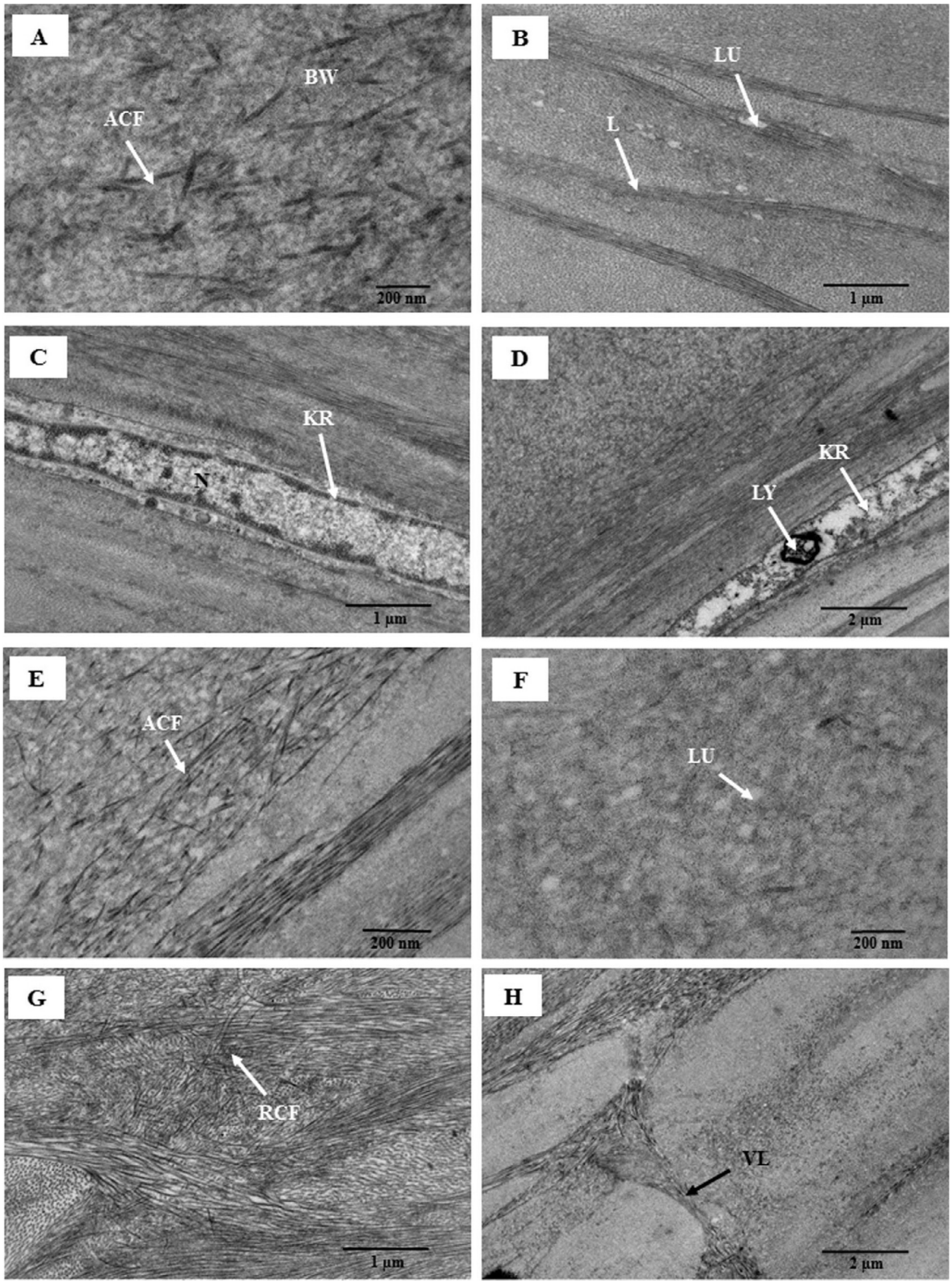

Fig. 2. Electron micrograph of the periphery and center of *Group 2* and *3* corneas; **A**) *Group 2*, periphery: abnormal long fibrils in the BW. **B**) *Group 2*, periphery: a normal healthy keratocyte with a large nucleus in the anterior stroma. **C**) *Group 2*, center: electron-lucent vacuoles in the anterior stroma. **D**) *Group 2*, center: a degenerated keratocyte with lysosomes in the anterior stroma. **E**) *Group 3*, periphery: abnormal collagen fibrils (CFs) in the Bowman layer (BW). **F**) *Group 3*, periphery: electron-lucent vacuoles and electron-dense material in the BW. **G**) *Group 3*, center: randomly running CFs in the anterior stroma. **H**) *Group 3*, center: vertically running lamellae between two parallel running lamellae in the anterior stroma. ACF, abnormal collagen fibril; BW, Bowman layer; F, folded lamellae; KR, keratocyte; LU, lucent spaces; L, lamellae; LY, lysosome; N, nucleus; RCF, randomly running collagen fibrils; VL, vertically running lamellae.

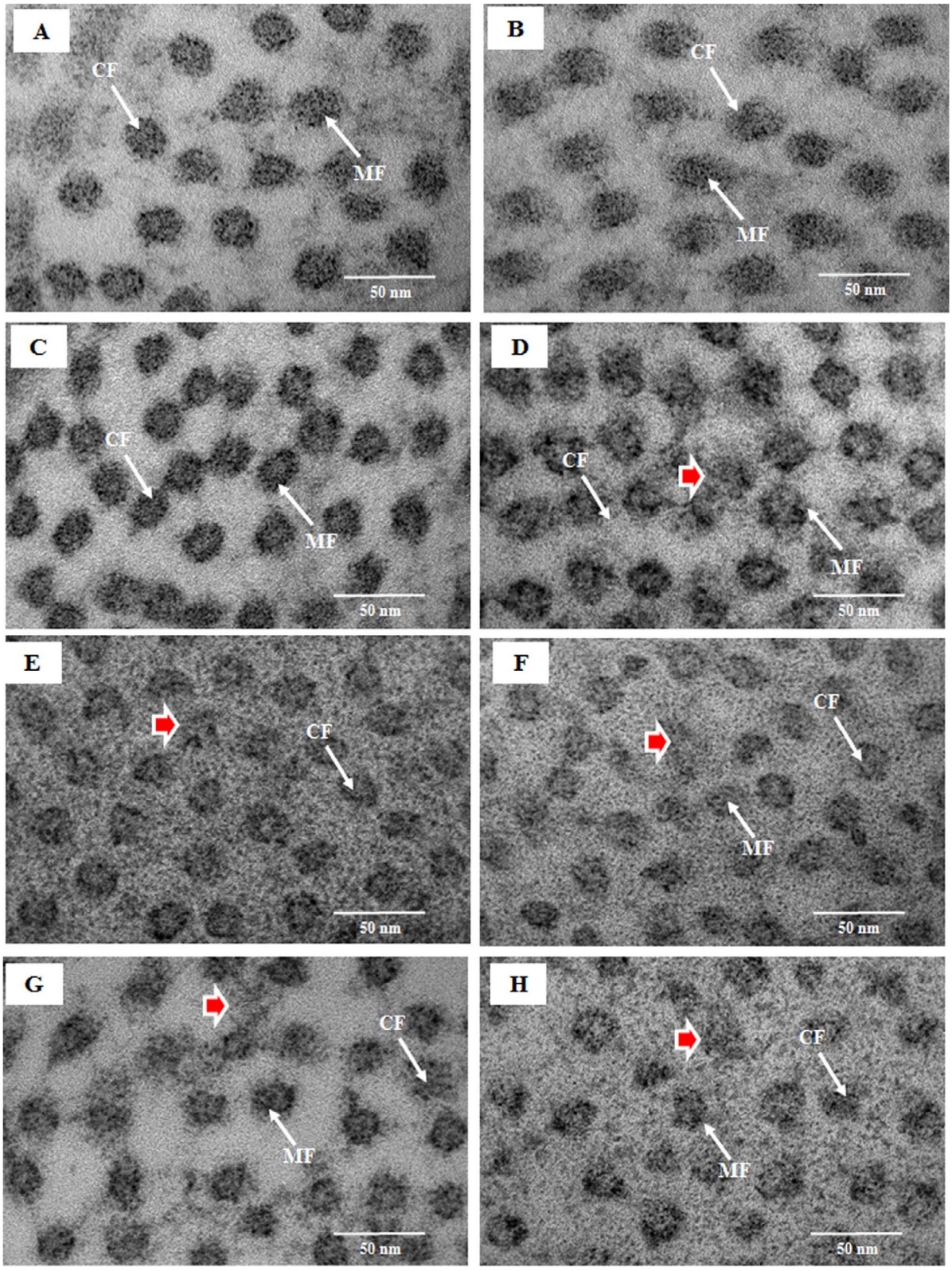

Fig. 3. Electron micrograph of collagen fibrils (CFs) of the periphery and center of *G0, G1, G2,* and *G3* corneas. **A**) *Group 1*, periphery: a normal healthy CF containing a large number of microfilaments surrounding the central lucent part. **B**) *Group 1*, center: the microfibrils within the CFs are less in number and not well-organized. **C**) *Group 2*, periphery: microfibrils within the CFs were fused to each other. **D**) *Group 2*, center: microfibrils within the CFs degenerated. **E**) *Group 3*, periphery: microfibrils within the CFs were distinguished but some CFs were degenerated (red arrow). **F**) *Group 3*, center: some CFs have microfibrils, whereas some lacked microfibrils. CF, collagen fibril; MCF, microfibrils within CF; red arrowhead, degenerated CF.

Table 1
Comparison of CF diameter, interfibrillar spacing, and density of CFs of anterior stroma of central and peripheral region of cornea treated with CXL and normal corneas, within the same CXL or normal cornea.

Groups	Cornea Zone	CF Diameter (nm)	CF Interfibrillar Spacing (nm)	Density/μm^2
Control	Center	23.32 ± 0.80 ** (n = 809)	36.98 ± 0.1 ** (n = 809)	535
	Periphery	23.37 ± 0.077 ** (n = 905)	35.90 ± 0.1 ** (n = 905)	598
	Center and periphery	23.60 ± 0.45 ** (n = 1714)	36.94 ± 0.10 ** (n = 1714)	566
Group 1	Centre	20.81 ± 0.13*,†, ** (n = 792)	35.14 ± 0.17*,†, ** (n = 792)	544
	Periphery	24.38 ± 0.11*,†,** (n = 814)	36.36 ± 0.15*,†, ** (n = 814)	537
	Center + Periphery	22.62 ± 0.097*,†, ** (n = 1606)	35.76 ± 0.11*,†,** (n = 1606)	541
Group 2	Center	18.80 ± 0.12*,†, ** (n = 1120)	29.68 ± 0.11*,†, ** (n = 1120)	740
	Periphery	21.37 ± 0.10*,†, ** (n = 1023)	31.64 ± 0.17*,†, ** (n = 1023)	676
	Center + Periphery	20.03 ± 0.08*,†, ** (n = 2143)	30.62 ± 0.10*,†, ** (n = 2143)	708
Group 3	Center	23.66 ± 0.10*,†, ** (n = 765)	37.21 ± 0.13*,†, ** (n = 765)	506
	Periphery	22.40 ± 0.11*,†, ** (n = 709)	37.25 ± 0.11*,†, ** (n = 709)	469
	Center and periphery	23.06 ± 0.07*,†, (n = 1474)	37.23 ± 0.12*,†, ** (n = 1474)	487

*: Significant difference ($p < 0.001$) compared between central and peripheral area in the same cornea (CXL or normal) (Mann-Whitney test).
†: Significant difference ($p < 0.001$) compared the same area of the cornea between the groups (Mann-Whitney test).
SE: Standard error.
**: Significant difference ($p < 0.001$) compared same area of the cornea between the group and the normal cornea (Mann-Whitney test).

and the microfilaments within the CFs were not differentiated both in the periphery and center (Fig. 2E, F). In *G3*, the structure of the microfilaments within the CFs was better organized in the periphery than that in the center (Fig. 2G, H). In both the peripheral and central parts, the microfibrils within the CFs showed signs of damage and were fused to each other (Fig. 3G, H). These ultrastructural changes could be due to the excess of water in the stroma.

3.2. CF diameter and interfibrillar spacing of the anterior stroma of normal and CXL-treated corneas

The analysis of CF diameter and interfibrillar spacing was performed by color-coding the monochrome images according to CF diameter. In the control group, the mean diameter of the CFs at the center (23.32 ± 0.80 nm) was approximately similar to that at the periphery (23.37 ± 0.07 nm) (Table 1 and Fig. 4A–D). The proportions of CFs with diameters between 20 and 30 nm at the center and periphery were 94.4% and 90.0%, respectively (Tables 1 and 2). In *G1*, in the central cornea, 58.7% of the CFs had diameters of between 20 and 30 nm, and the mean diameter of all CFs was 20.81 ± 0.13 nm (Fig. 4E, F and Tables 1 and 2), whereas in the peripheral cornea, 93.90% of the CFs had diameters between 20 and 30 nm, and the mean diameter of all CFs was 24.38 ± 0.1 1 nm (Fig. 4G, H and Tables 1 and 2). In *G2*, CFs with diameters in the range of 20–30 nm accounted for 33.30% of all CFs in the central cornea, and the mean CF diameter was 18.80 ± 0.12 nm, whereas in the periphery, 69.60% of the CFs had diameters between 20 and 30 nm, and the mean CF diameter was 21.3 ± 0. 10 nm (Fig. 5A–D and Tables 1 and 2). In both *G1* and *G2*, the mean diameter of the central CFs was significantly smaller than that of the peripheral CFs (Table 1). In *G3*, where UVA was not used, the mean CF diameter (23.66 ± 0.10 nm) at the center was larger than that at the periphery (22.40 ± 0.11 nm) (Fig. 5E–H and Table 1). In addition, more CFs with diameters in the range of 20–30 nm were observed at the center (91.40%) than at the periphery of the cornea (82.70%) (Tables 1 and 2). In *G1* and *G2*, the interfibrillar spacing of the peripheral cornea was larger than that of the central cornea, whereas in *G3*, no difference was observed between the central and peripheral corneas (Table 1). Among the groups, the interfibrillar spacing of the corneal stroma in *G2* was significantly smaller than that in *G1*. The interfibrillar spacing in *G3* was larger than those in both *G1* and *G2* (Table 1). No significant difference in the density of the CFs was observed between all groups.

3.3. Mean PG area and density of normal and CXL-treated corneas

The mean PG area was obtained by color-coding the electron micrographs according to the area of the PGs (Figs. 6 and 7). The PGs were normally distributed in the center and periphery of the normal corneas in the control group. In *G1*, the mean PG area (98.31 ± 1.5 nm^2) in the center was significantly larger than that in the periphery (74.53 ± 0.90 nm^2), whereas the density of the PGs in the center (408/μm^2) was smaller than that in the periphery (591/μm^2) (Table 3). In *G2*, the mean PG area in the center (83.03 ± 1.13 nm^2) was significantly smaller than that in the periphery (96.20 ± 1.60 nm^2). In *G3*, the mean PG area in the center was also smaller than that in the periphery (Table 3). In *G1* and *G3*, the PGs in the center were denser than those in the periphery (Table 3). Between the groups, the mean PG areas in *G0* and *G2* were significantly larger than those in *G1* and *G3* ($p < 0.0001$). The PGs in *G1* and *G3* were denser than those in *G2* (Table 3).

4. Discussion

Iontophoresis has been widely and successfully used for the application of riboflavin in CXL treatment (Eljarrat-Binstock et al., 2004; Mencucci et al., 2015; Vinciguerra et al., 2013). In this study, iontophoresis was used for the uniform distribution of riboflavin in

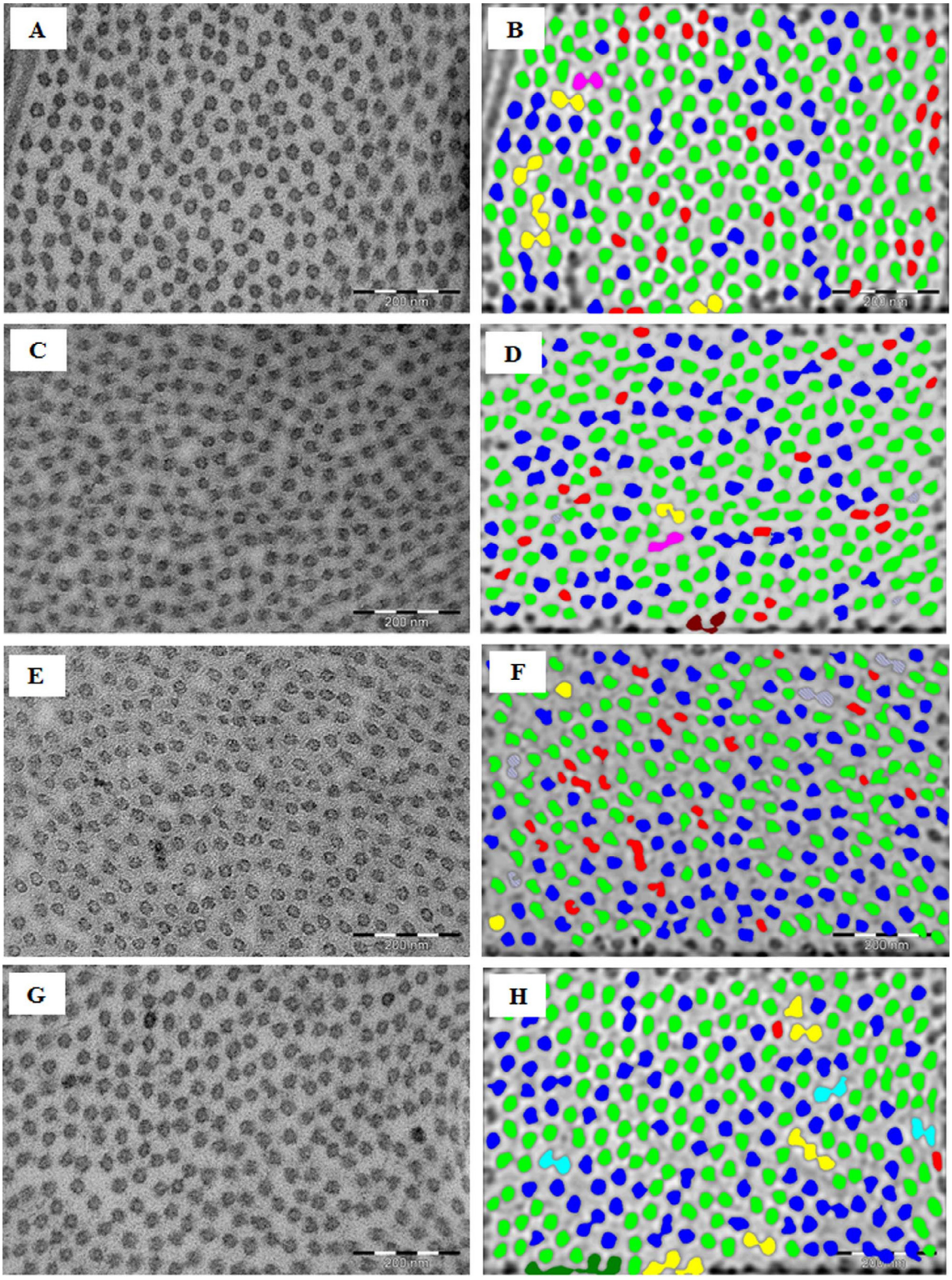

Fig. 4. Monochrome electron micrographs and color-coded digital images of the periphery and center of *G0* and *G1* corneas. **A)** Monochrome micrograph of collagen fibrils (**CFs**) of the anterior stroma of the central part of a *G0* cornea. **B) A** color-coded image of "Figure A" containing mostly green (15–20 nm) and blue (20–25 nm) and few yellow (25–30 nm) CFs (osmium tetroxide fixation). **C)** Monochrome micrograph of **CFs** of the anterior stroma of the peripheral part of a *G0* cornea. **D)** A color-coded image of "Figure C" containing mostly green (15–20 nm) and blue (20–25 nm) CFs (osmium tetroxide fixation). **E)** Monochrome micrograph of **CFs** of the anterior stroma of the central part of a *G1* cornea. **F)** A color-coded image of "Figure E" containing mostly green (15–20 nm) and blue (20–25 nm) CFs (osmium tetroxide fixation). **G)** Monochrome micrograph of **CFs** of the anterior stroma of the peripheral part of a *G1* cornea. **H)** A color-coded image of "Figure G" containing mostly green (15–20 nm) and blue (20–25 nm) and few yellow (25–30 nm) CFs (osmium tetroxide fixation).Red, 10–20 nm; Green, 15–20 nm; Blue, 20–25 nm; Yellow, 25–30 nm; Terracotta, 30–35 nm.

Table 2
Cross tabulation of CFs diameter percentage of the center and peripheral cornea of Group 1, 2 and 3.

	CFs Diameters (%)					
		10–15 nm	15–20 nm	20–25 nm	25–30 nm	30–35 nm
Control	Center	0.0	5.2	77.4	16.9	0.5
	Periphery	0.0	4.9	**78.3**	**15.7**	1.1
Group 1	Center	6.2	33.5	50.9	7.8	1.5
	Periphery	0.0	4.7	**56.1**	**37.8**	1.4
Group 2	Center	13.8	52.2	31.7	1.6	0.7
	Periphery	3.1	27.1	**62.6**	7.0	0.3
Group 3	Center	0.9	6.8	63.6	**27.8**	0.9
	Periphery	0.0	17.2	**68.2**	14.5	0.1

the *ex vivo* corneal culture for 5 min, followed by UVA irradiation as follows: 1) UVA with irradiance of 3 mW/cm^2 for 30 min (*G1*); 2) UVA irradiance of 10 mW/cm^2 for 9 min (*G2*); 3) without UVA irradiation (*G3*); 4) control (*G0*). The main objective of this study was to assess the efficacy of CXL in the aforementioned groups at the center and periphery of the same corneal button.

4.1. Ultrastructural changes in the center and periphery of corneas from the analyzed groups

Ultrastructure studies have revealed that healthy and untreated corneas of the control group (*G0*) contained well-organized and interconnected lamellae in the anterior stroma and parallel running lamellae in the posterior stroma of central and peripheral corneas. The interconnection between the lamellae in the anterior stroma is essential for corneal biomechanical properties, including rigidity, shape, and curvature (Winkler et al., 2013). In *G3*, this essential property of lamellar interconnectivity has been disturbed, and the lamellae were running randomly and vertically in both central and peripheral corneas. This disorganization of the lamellae could be due to excess hydration or water content around the CFs, caused by the application of riboflavin without UVA radiation. The interconnectivity and organization of the lamellae in the anterior stroma in *G1* and *G2* were evenly laid out. Occasional folding of irregular lamellae in the central stroma may be caused by the high intensity of radiation on an individual CF. The peripheral part of the cornea had a better stromal architecture than the central part of the cornea; however, it was better preserved in *G1*. The peripheral cornea in *G2* contained healthy-looking keratocytes, contradictory to the observation of Wollensak et al. (2004b), who have reported the toxicity of UVA irradiation (range of 0.5–0.7 mW/cm^2) toward keratocytes in rabbit eyes enucleated 24 h after treatment (Mencucci et al., 2010). However, the application of longer-duration UVA irradiation resulted in visible damage to keratocytes in the peripheral cornea. Regarding cytotoxic damage related to CXL, it seems that the exposure duration is the deciding factor rather than the energy applied.

4.2. Within the same cornea of G1, G2, and G3: CF diameter and interfibrillar spacing in the center and periphery

X-ray diffraction studies of normal cornea have reported that CF diameters of healthy central and peripheral corneas were not significantly different; however, the interfibrillar spacing in the center was smaller than that in the periphery (Boote et al., 2003). Authors have believed that the compactness of the CFs contributes to more rigid biomechanical and stress-bearing properties of the central cornea (Boote et al., 2003). In addition, the compactness of the CFs provides strength to maintain the curvature of the cornea (Boote et al., 2003).

In this study, the diameter, spacing, and density of the CFs in the center and periphery of the normal cornea were not significantly different. In *G3*, where the riboflavin solution was applied without irradiation, the CF diameter in the center was larger than that in the periphery of the cornea. It could be possible that the riboflavin and water absorption by the CFs might have occurred more at the central part of the cornea than at the peripheral aspect of the cornea. Due to the lack of UVA, there might be no CXL between the collagen molecules and core proteins and between CFs and core proteins. The increase in the diameter may be due to an increase in hydration within the CFs.

In *G1* and *G2*, CF diameters and interfibrillar spacing in the periphery were significantly larger than those in the center. Moreover, the application of higher UVA irradiance in *G2* resulted in visible damage to the CFs not only in the center but also in the periphery, whereas *G1* exhibited CF damage only in the central region. Zang et al. (2011) have reported that in CXL-treated corneas, collagen molecules cross-link themselves, similarly as the PG core proteins. In addition, a linkage existed between collagen and two specific core proteins, mimican and decorin. When both collagen and PG core proteins are present together in a solution, the corneal PG core proteins, keratocan and lumican, inhibit collagen CXL. However, mimican and decorin cross-links with collagen to form a new high-molecular-weight polymer. In the absence of riboflavin + UVA, the linkage between collagen and keratocan and lumican was different from that between collagen and mimican and decorin (Zang et al., 2011). The reaction of the CFs to riboflavin–CXL (in *G1* and *G2*) may be related to their structure and arrangement at the periphery or center of the cornea. The presence of collagen proteins and PGs within the CFs may contribute to the absorption of riboflavin and UVA. The increase in the diameter may be due to a rise in microfilament content within the CFs due to the CXL of core proteins keratocan and lumican of glycosaminoglycan chain with collagen proteins (Zang et al., 2011).

4.3. Among the corneas of G1, G2, and G3: CF diameter and interfibrillar spacing

Riboflavin–UVA treatment increased the CF diameter in the anterior stroma compared with that in the normal corneal stroma of rabbit cornea (Wollensak et al., 2004a). The lamellar organization and CF diameter of the corneoscleral strip also increased after the riboflavin–UVA treatment (Choi et al., 2013). The CF diameter and interfibrillar spacing, as well as the ultrastructure of the KC cornea, increased after the riboflavin–UVA treatment (Akhtar et al., 2013). In this study, not only the ultrastructure of the cornea treated with riboflavin + 3 mW/cm^2 irradiance for 30 min (*G1*) but also the CF diameter and interfibrillar spacing were similar to those of the normal cornea in the control group.

In *G2*, the reduction in the diameter and close packing of the CFs could be due to evaporation of the water content, denaturation CF proteins, and reduced imbibition of the riboflavin related to the delivered energy rather than the duration of irradiance. Although the CF diameter and interfibrillar spacing of the cornea treated

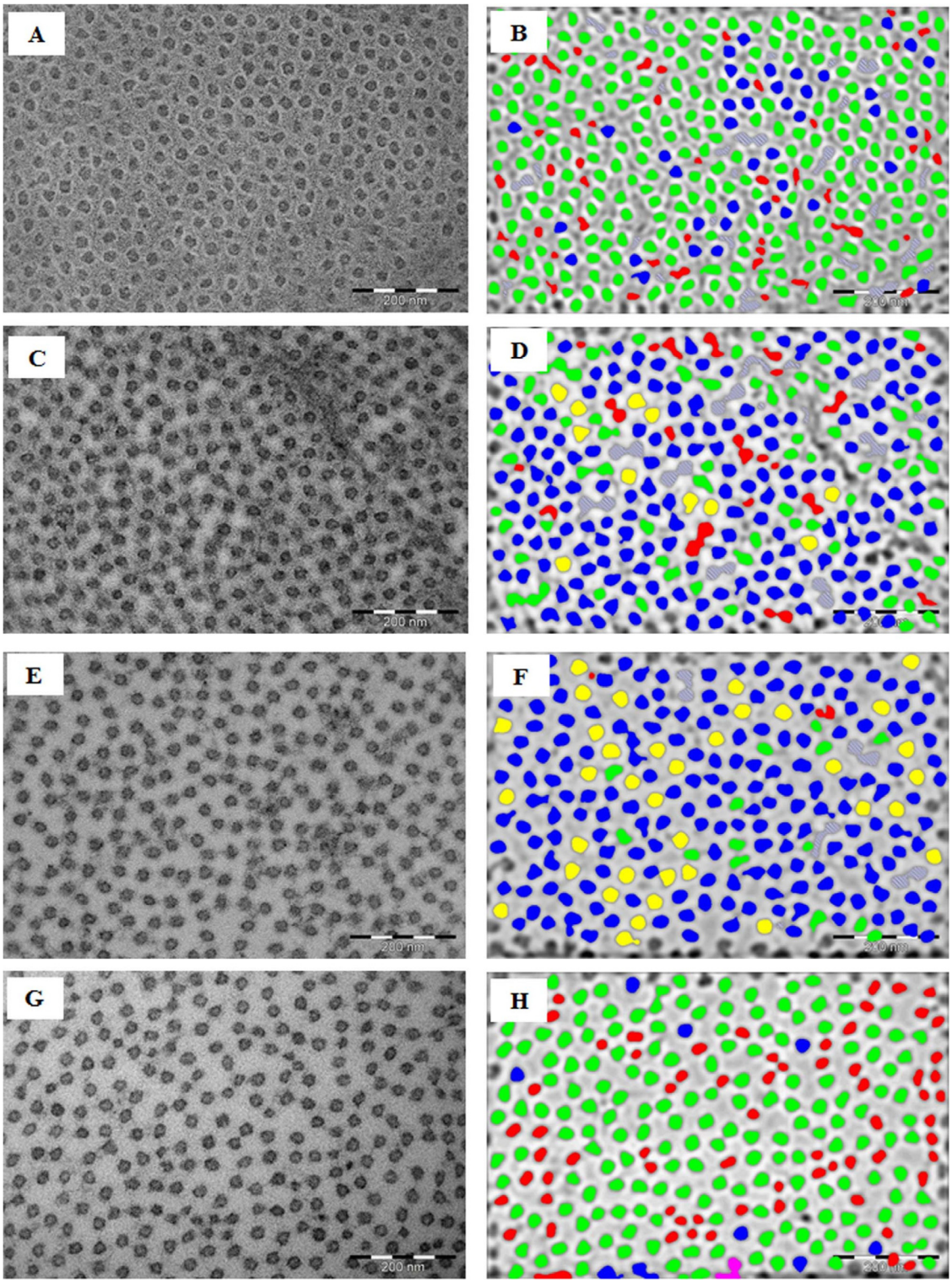

Fig. 5. Monochrome electron micrographs and color-coded digital images of the periphery and center of *G2* and *G3* corneas. **A**) Monochrome micrograph of CFs of the anterior stroma of the central part of a *G2* cornea. **B**) Color-coded image of "Figure A" containing mostly green (15–20 nm) and few red (10–15 nm) and blue (20–25 nm) color-coded CFs (osmium tetroxide fixation). **C**) Monochrome micrograph of CFs of the anterior stroma of the peripheral part of a *G2* cornea. **D**) Color-coded image of "Figure C" containing mostly blue (20–25 nm) and few red (10–15 nm), green (15–20 nm), and yellow (25–30 nm) color-coded CFs (osmium tetroxide fixation). **E)** Monochrome micrograph of **CFs** of the anterior stroma of the central part of a *G3* cornea. **F)** Color-coded image of "Figure E" containing mostly blue (20–25 nm) and yellow (25–30 nm) color-coded CFs (osmium tetroxide fixation). **G)** Monochrome micrograph of CFs of the anterior stroma of the peripheral part of a ***G3*** cornea. **H)** Color-coded image of "Figure G" containing mostly red (10–15 nm) and green (20–25 nm) color-coded CFs. Red, 10–20 nm; Green, 15–20 nm; Blue, 20–25 nm; Yellow, 25–30 nm; Terracotta, 30–35 nm.

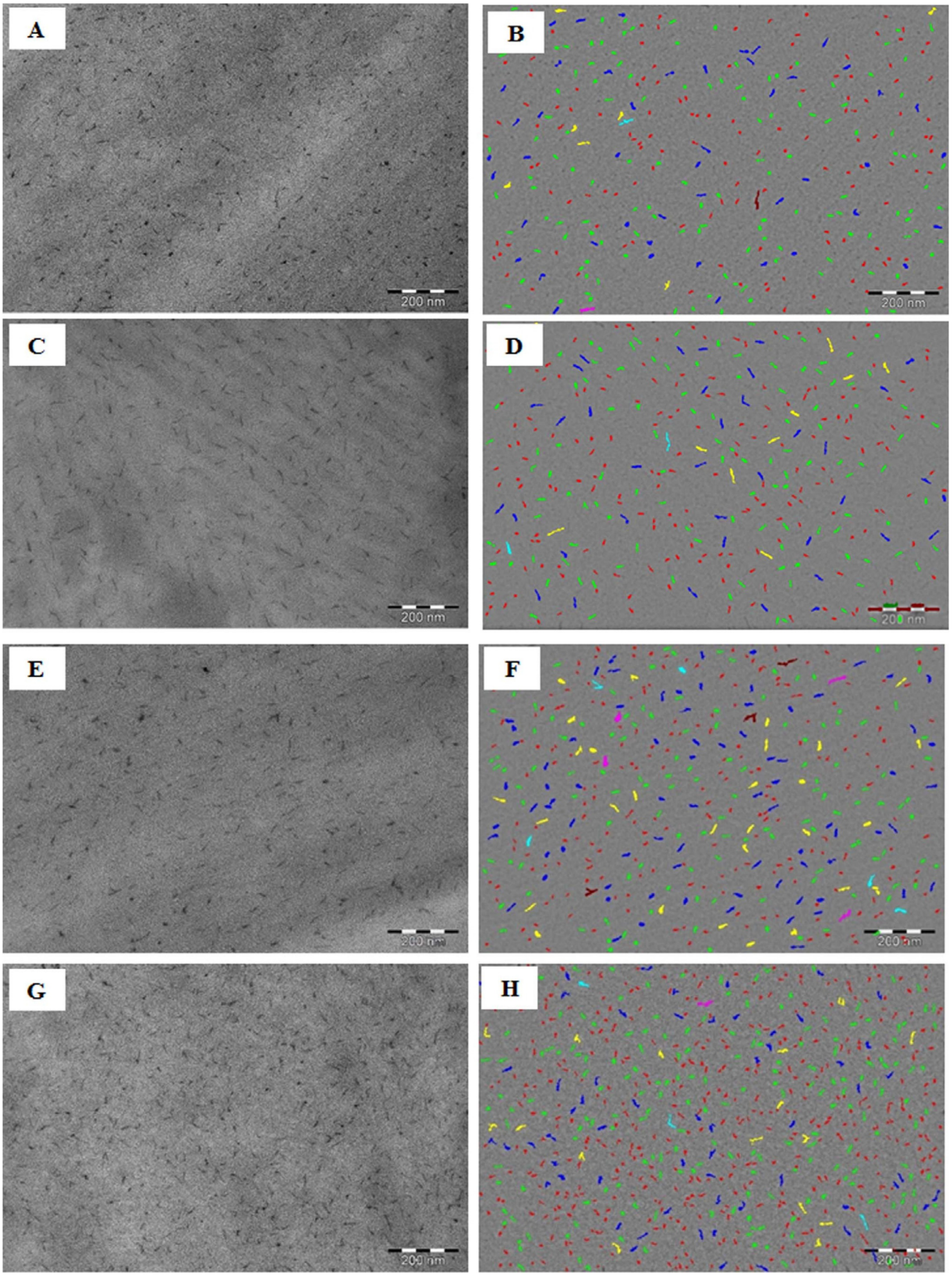
A
200 nm
B
200 nm
C
200 nm
D
200 nm
E
200 nm
F
200 nm
G
200 nm
H
200 nm

Fig. 6. Monochrome electron micrographs and digital color-coded images of proteoglycans in *G0 and G1* corneas. A) Monochrome micrograph of the anterior stroma of the central part of a *G0* cornea. **B**) Color-coded image of "Figure A" containing mostly green, blue, and brown PGs. **C)** Monochrome micrograph of the anterior stroma of the peripheral part of a *G0* cornea. **D**) Color-coded image of "Figure C" containing mostly brown and green and few blue and yellow PGs. **E**) Monochrome micrograph of the anterior stroma of the central part of a *G1* cornea. **F**) Color-coded image of "Figure E" containing mostly green, brown, and blue PGs. **G)** *G1* monochrome micrograph of the anterior stroma of the peripheral part of a *G1* cornea. **H)** Color-coded image of "Figure G" containing mostly green, blue, and brown and few yellow and terracotta PGs.Red, 30–80 nm^2; Green, 80–130 nm^2; Blue, 130–180 nm^2; Yellow, 180–230 nm^2; Terracotta, 230–280 nm^2; Pink, 280–330 nm^2; Brown, 330–380 nm^2.

with riboflavin without UVA (*G3*) were similar to those of the normal cornea, the structure of the stroma has been impaired. The increase in CF diameter and interfibrillar spacing could be due to the high water content within the CFs. The analysis of the CF diameter and interfibrillar spacing alone will be misleading to assess the effects of riboflavin on the cornea.

The overall density of PGs in *G1* was higher than those in other groups. The PGs in *G1, G2,* and *G3* reacted differently according to the intensity of UVA treatment. The linkages among the glycosylated core proteins might have been affected by the use of CXL treatment using different irradiances of UVA for different durations, resulting in variations in PG density at the peripheral and central parts of the cornea.

In conclusion to our results, an obvious difference in the phototoxic effect was observed related to different CXL settings. Long exposure with smaller UVA irradiance seems to have a less pronounced phototoxic effect on acellular corneal structures (CFs and PGs), which is mostly limited to the central corneal region. In contrast to this, the impact on cellular corneal compound (keratocytes) is more severe in this group and results in keratocyte damage visible in both the central and peripheral cornea. Short exposure with higher UVA irradiance has a much stronger phototoxic effect on acellular compounds (CFs and PGs), which is observed in both the central and peripheral parts of the cornea, which is accompanied by a lower cytotoxic effect toward corneal keratocytes (especially in the peripheral cornea). The lower cytotoxic effect toward keratocytes may predict a better healing process after CXL treatment.

The discrepancies between the effects of CXL on the central and peripheral parts of the cornea may be explained lateral diffusion of oxygen. It could be possible that there is a higher oxygen content at the periphery of the cornea due to lateral diffusion of the oxygen from the un-irradiated area. Seiler et al. (2020) measured the oxygen in the center at several depths. In the center the oxygen is depleted through the UV irradiation and reaches only 1–2 % within the cornea. In the periphery the oxygen can diffuse through the un-irradiated area and reaches about 18% at 100 μm, 15 % at 200 μm, and 14 % at 300 μm. Such a high oxygen gradient between the irradiated and un-irradiated part of the cornea leads to a suction of oxygen into the irradiated area. The periphery of the irradiated cornea gets more oxygen and the CXL effect may be stronger due to the laterally diffused oxygen. In addition to that, a "higher peripheral intensity" is more effective compared to the "top hat" profile on the topographic and tomographic parameters of the cornea during the CXL treatment (Herber et al, 2018).

Hence, we believe that the application of riboflavin + UVA reacted differently to the CFs at the center and periphery. Based on CXL's reaction at the periphery and center, the linkages among the collagen molecules and those among the core proteins vary, resulting in variations in the microfibrils within the CFs, CF diameter, and interfibrillar spacing. Based on this study, we believe that the application of riboflavin + UVA at 3 mW/cm^2 for 30 min and 10 mW/cm^2 for 9 min is a suitable method of CXL; however, the application at 3 mW/cm^2 for 30 min improved the organization and size of the collagen fibrils. CXL treatment applied at the periphery was more effective than that applied at the center.

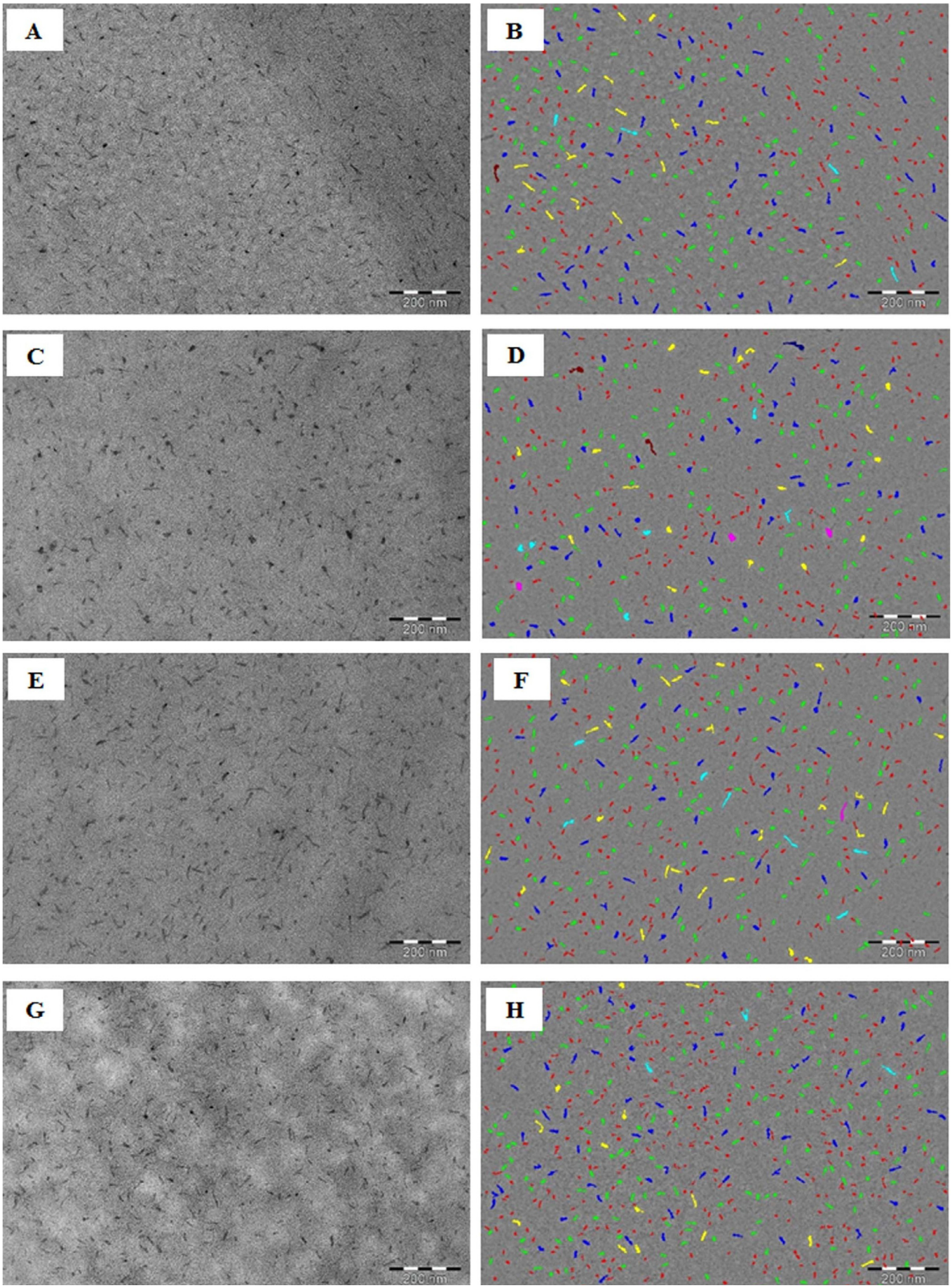
A
200 nm
B
200 nm
C
200 nm
D
200 nm
E
200 nm
F
200 nm
G
200 nm
H
200 nm

Fig. 7. Monochrome electron micrographs and digital color-coded images of proteoglycans in *G2 and G3* corneas. A) Monochrome micrograph of the anterior stroma of the central part of a *G2* cornea. **B**) Color-coded image of "Figure A" containing mostly green, blue, and terracotta PGs. **C)** Monochrome micrograph of the anterior stroma of the peripheral part of a *G2* cornea. **D)** Color-coded image of "Figure C" containing mostly brown, green, and blue and few yellow and terracotta PGs. **E**) Monochrome micrograph of the anterior stroma of the central part of a *G3* cornea. **F**) Color-coded image of "Figure E" containing mostly green, brown, and terracotta PGs. **G)** Monochrome micrograph of the anterior stroma of the peripheral part of a *G3* cornea. **H)** Color-coded image of "Figure G" containing mostly brown, green, and blue and few yellow and terracotta PGs. Red, 30–80 nm^2; Green, 80–130 nm^2; Blue, 130–180 nm^2; Yellow, 180–230 nm^2; Terracotta, 230–280 nm^2; Pink, 280–330 nm^2; Brown, 330–380 nm^2.

Table 3
Comparison of proteoglycans area, and density of PGs in the anterior stroma of central and peripheral within the same CXL treated cornea or normal cornea.

Groups		Central Cornea	Periphery Cornea	Center + Periphery Cornea
Control	PGs Area (nm^2) Density/ μm^2	90.97 ± 0.80*,†, **(n = 1004) 289	97.14 ± 0.46(n = 1098) 316	94.05 ± 0.63(n= 2102) 605
Group 1	PGs Area (nm^2) Density /μm^2	98.31 ± 1.5*,†, ** (n = 1406) 408	74.53 ± 0.90 (n = 2039) 591	84.23 ± 0.84 (n = 3445) 999
Group 2	PGs Area (nm^2) Density/ μm^2	83.03 ± 1.13*,†, ** (n = 1515) 439	96.20 ± 1.60 (n = 1336) 387	89.20 ± 0.97 (n = 2851) 826
Group 3	PGs Area (nm^2) Density/ μm^2	81.40 ± 1.14*,†, ** (n = 1572) 455	87.37 ± 1.17 (n = 1852) 536	84.63 ± 0.82 (n = 3424) 992

*: Significant difference ($p < 0.001$) compared between central and peripheral area in the same cornea (CXL or normal) (Mann-Whitney test).
†: Significant difference ($p < 0.001$) compared the same area of the cornea between the groups (Mann-Whitney test).
SE: Standard error.
**: Significant difference ($p < 0.001$) compared same area of the cornea between the group and the normal cornea (Mann-Whitney test).

Declaration of Competing Interest

The authors declare that they have no known competing financial interests or personal relationships that could have appeared to influence the work reported in this paper.

Acknowledgments

This research project was funded by the National Plan for Science and Technology Program (Grant Number 15MED4229-02), King Saud University, Riyadh, Saudi Arabia.

The authors thank the Deanship of Scientific Research and RSSU of King Saud University for their technical support.

References

Akhtar, S., Alkhalaf, M., Khan, A.A., Almubrad, T.M., 2016. Ultrastructure features and three-dimensional transmission electron tomography of Dhub Lizard (Uromastyx aegyptia) cornea and its adaptation to a desert environment. Microsc. Microanal. 22 (4), 922–932.

Akhtar, S., Almubrad, T., Paladini, I., Mencucci, R., 2013. Keratoconus corneal architecture after riboflavin/ultraviolet A cross-linking: ultrastructural studies. Mol. Vis. 19, 1526–1537.

Akhtar, S., Bron, A.J., Hayes, A.J., Meek, K.M., Caterson, B., 2011. Role of keratan sulphate (sulphated poly -N-acetyllactosamine repeats) in keratoconic cornea, histochemical, and ultrastructural analysis. Graefes Arch. Clin. Exp. Ophthalmol. 249 (3), 413–420.

Akhtar, S., Bron, A.J., Salvi, S.M., Hawksworth, N.R., Tuft, S.J., Meek, K.M., 2008. Ultrastructural analysis of collagen fibrils and proteoglycans in keratoconus. Acta Ophthalmol. 86, 764–772.

Belin, M.W., Lim, L., Rajpal, R.K., Hafezi, F., Gomes, J.A.P., Cochener, B., 2018. Corneal cross-linking: current USA status: report from the Cornea Society. Cornea 37, 1218–1225.

Boote, C., Dennis, S., Newton, R.H., Puri, H., Meek, K.M., 2003. Collagen fibrils appear more closely packed in the prepupillary cornea: optical and biomechanical implications. Invest. Ophthalmol. Vis. Sci. 44 (7), 2941. https://doi.org/10.1167/iovs.03-0131.

Bredrup, C., Knappskog, P.M., Majewski, J., Rødahl, E., Boman, H., 2005. Congenital stromal dystrophy of the cornea caused by a mutation in the decorin gene. Invest. Ophthalmol. Vis. Sci. 46 (2), 420. https://doi.org/10.1167/iovs.04-0804.

Chaerkady, R., Shao, H., Scott, S.-G., Pandey, A., Jun, A.S., Chakravarti, S., 2013. The keratoconus corneal proteome: loss of epithelial integrity and stromal degeneration. J. Proteomics 87, 122–131.

Cheng, X.i., Pinsky, P.M., 2013. Mechanisms of self-organization for the collagen fibril lattice in the human cornea. J. R. Soc. Interface 10 (87), 20130512. https://doi.org/10.1098/rsif.2013.0512.

Choi, S., Lee, S.-C., Lee, H.-J., Cheong, Y., Jung, G.-B., Jin, K.-H., Park, H.-K., 2013. Structural response of human corneal and scleral tissues to collagen cross-linking treatment with riboflavin and ultraviolet A light. Lasers Med. Sci. 28 (5), 1289–1296.

Eljarrat-Binstock, E., Raiskup, F., Frucht-Pery, J., Domb, A.J., 2004. Hydrogel probe for iontophoresis drug delivery to the eye. J. Biomater. Sci. Polym. Ed. 15 (4), 397–413.

Fullwood, N.J., Tuft, S.J., Malik, N.S., Meek, K.M., Ridgway, A.E., Harrison, R.J., 1992. Synchrotron x-ray diffraction studies of keratoconus corneal stroma. Invest. Ophthalmol. Vis. Sci. 33, 1734–1741.

Funderburgh, J.L., Conrad, G.W., 1990. Isoforms of corneal keratan sulfate proteoglycan. J. Biol. Chem. 265 (14), 8297–8303.

Ho, L.T.Y., Harris, A.M., Tanioka, H., Yagi, N., Kinoshita, S., Caterson, B., Quantock, A.J., Young, R.D., Meek, K.M., 2014. A comparison of glycosaminoglycan distributions, keratan sulphate sulphation patterns and collagen fibril architecture from central to peripheral regions of the bovine cornea. Matrix Biol. 38, 59–68.

Manetti, M., Favuzza, E., Sgambati, E., Mencucci, R., Marini, M., 2017. A case of in vivo iontophoresis-assisted corneal collagen cross-linking for keratoconus: an immunohistochemical study. Acta Histochem. 119 (3), 343–347.

Mazzotta, C., Traversi, C., Baiocchi, S., Bagaglia, S., Caporossi, O., Villano, A., Caporossi, A., 2018. Corneal collagen cross-linking with riboflavin and ultraviolet A light for pediatric keratoconus: ten-year results. Cornea 37, 560–566.

Mazzotta, C., Traversi, C., Baiocchi, S., Caporossi, O., Bovone, C., Sparano, M.C., Balestrazzi, A., Caporossi, A., 2008. Corneal healing after riboflavin ultraviolet-A

collagen cross-linking determined by confocal laser scanning microscopy in vivo: early and late modifications. Am. J. Ophthalmol. 146 (4), 527–533.e1.
Mencucci, R., Ambrosini, S., Paladini, I., Favuzza, E., Boccalini, C., Raugei, G., Vannelli, G.B., Marini, M., 2015. Early effects of corneal collagen cross-linking by iontophoresis in ex vivo human corneas. Graefes Arch. Clin. Exp. Ophthalmol. 253 (2), 277–286.
Mencucci, R., Marini, M., Paladini, I., Sarchielli, E., Sgambati, E., Menchini, U., Vannelli, G.B., 2010. Effects of riboflavin/UVA corneal cross-linking on keratocytes and collagen fibres in human cornea. Clin. Exp. Ophthalmol. 38, 49–56.
Nautscher, N., Bauer, A., Steffl, M., Amselgruber, W.M., 2016. Comparative morphological evaluation of domestic animal cornea. Vet. Ophthalmol. 19 (4), 297–304.
O'Brart, D.P.S., Patel, P., Lascaratos, G., Wagh, V.K., Tam, C., Lee, J., O'Brart, N.A., 2015. Corneal cross-linking to halt the progression of keratoconus and corneal ectasia: seven-year follow-up. Am. J. Ophthalmol. 160 (6), 1154–1163.
Pellegata, N.S., Dieguez-Lucena, J.L., Joensuu, T., Lau, S., Montgomery, K.T., Krahe, R., Kivelä, T., Kucherlapati, R., Forsius, H., de la Chapelle, A., 2000. Mutations in KERA, encoding keratocan, cause cornea plana. Nat. Genet. 25 (1), 91–95.
Rabinowitz, Y.S., 1998. Keratoconus. Surv. Ophthalmol. 42 (4), 297–319.
Herber, R., Kunert, K.S., Velika, V., Spoerl, E., Pillunat, L.E., Raiskup, F., 2018. Influence of the beam profile crosslinking setting on changes in corneal topography and tomography in progressive keratoconus. J. Cataract Refract. Surg. 44, 718–724.
Sawaguchi, S., Yue, B.Y., Chang, I., Sugar, J., Robin, J., 1991. Proteoglycan molecules in keratoconus corneas. Invest. Ophthalmol. Vis. Sci. 32, 1846–1853.
Seiler, T.G., Komninou, M.A., Nambiar, M.H., Schuerch, K., Frueh, B.E., Büchler, P., 2021. Oxygen kinetics during corneal cross-linking with and without supplementary oxygen. Am. J. Ophthalmol. 223, 368–376.
Sharif, R., Fowler, B., Karamichos, D., Mohan, R.R., 2018. Collagen cross-linking impact on keratoconus extracellular matrix. PLoS ONE 13 (7), e0200704. https://doi.org/10.1371/journal.pone.020070410.1371/journal.pone.0200704.g001.
Vinciguerra, P., Randleman, J.B., Romano, V., Legrottaglie, E.F., Rosetta, P., Camesasca, F.I., Piscopo, R., Azzolini, C., Vinciguerra, R., 2014. Transepithelial iontophoresis corneal collagen cross-linking for progressive keratoconus: initial clinical outcomes. J. Refract. Surg. 30 (11), 746–753.
Vinciguerra, P., Rechichi, M., Rosetta, P., Romano, M.R., Mastropasqua, L., Scorcia, V., Azzolini, C., Vinciguerra, R., 2013. High fluence iontophoretic corneal collagen cross-linking: in vivo OCT imaging of riboflavin penetration. J. Refract. Surg. 29 (6), 376–377.
Wernli, J., Schumacher, S., Spoerl, E., Mrochen, M., 2013. The efficacy of corneal cross-linking shows a sudden decrease with very high intensity UV light and short treatment time. Invest. Ophthalmol. Vis. Sci. 54 (2), 1176. https://doi.org/10.1167/iovs.12-11409.
Winkler, M., Shoa, G., Xie, Y., Petsche, S.J., Pinsky, P.M., Juhasz, T., Brown, D.J., Jester, J.V., 2013. Three-dimensional distribution of transverse collagen fibers in the anterior human corneal stroma. Invest. Ophthalmol. Vis. Sci. 54 (12), 7293. https://doi.org/10.1167/iovs.13-13150.
Wollensak, G., Spoerl, E., Seiler, T., 2003a. Riboflavin/ultraviolet-a-induced collagen crosslinking for the treatment of keratoconus. Am. J. Ophthalmol. 135 (5), 620–627.
Wollensak, G., Spoerl, E., Seiler, T., 2003b. Stress-strain measurements of human and porcine corneas after riboflavin-ultraviolet-A-induced cross-linking. J. Cataract Refract. Surg. 29, 1780–1785.
Wollensak, G., Spoerl, E., Wilsch, M., Seiler, T., 2004a. Keratocyte apoptosis after corneal collagen cross-linking using riboflavin/UVA treatment. Cornea 23 (1), 43–49.
Wollensak, G., Sporl, E., Mazzotta, C., Kalinski, T., Sel, S., 2011. Interlamellar cohesion after corneal crosslinking using riboflavin and ultraviolet A light. Br. J. Ophthalmol. 95 (6), 876–880.
Wollensak, G., Wilsch, M., Spoerl, E., Seiler, T., 2004b. Collagen fiber diameter in the rabbit cornea after collagen crosslinking by riboflavin/UVA. Cornea 23 (5), 503–507.
Wollensak, J., Buddecke, E., 1990. Biochemical studies on human corneal proteoglycans–a comparison of normal and keratoconic eyes. Graefes Arch. Clin. Exp. Ophthalmol. 228 (6), 517–523.
Zang, L.i., Frenkel, R., Simeone, J., Lanan, M., Byers, M., Lyubarskaya, Y., 2011. Metabolomics profiling of cell culture media leading to the identification of riboflavin photosensitized degradation of tryptophan causing slow growth in cell culture. Anal. Chem. 83 (13), 5422–5430.